

$\pi N \rightarrow \omega N$ in a Coupled-Channel Approach[†]

G. Penner* and U. Mosel

Institut für Theoretische Physik, Universität Giessen, D-35392 Giessen

We describe the $\pi N \rightarrow \omega N$ cross section from threshold to a center of mass energy of 2 GeV in a unitary coupled-channel model and analyze it in terms of rescattering and resonance excitations. The amplitude is mainly composed of D_{13} , P_{13} , and P_{11} contributions, where the D_{13} dominates over the complete considered energy range. We also outline the generalization of the standard partial-wave formalism necessary for the decomposition of the ωN final state.

PACS numbers: 11.80.Gw,13.75.Gx,11.80.Et,14.20.Gk

I. INTRODUCTION

The reliable extraction of nucleon resonance properties from experiments where the nucleon is excited either via hadronic or electromagnetic probes is one of the major issues of hadron physics. The goal is to be finally able to compare the extracted masses and partial decay widths to predictions from lattice QCD (e.g. [1]) and/or quark models (e.g. [2, 3]).

With this aim in mind we developed in [4] a unitary coupled-channel effective Lagrangian model that already incorporated the final states γN , πN , $2\pi N$, ηN , and $K\Lambda$ and was used for a simultaneous analysis of all available experimental data on photon- and pion-induced reactions on the nucleon.

In an extension of the model to higher c.m. energies, i.e. up to center of mass energies of $\sqrt{s} = 2$ GeV for the investigation of higher and so called hidden nucleon resonances, the consideration of other final states

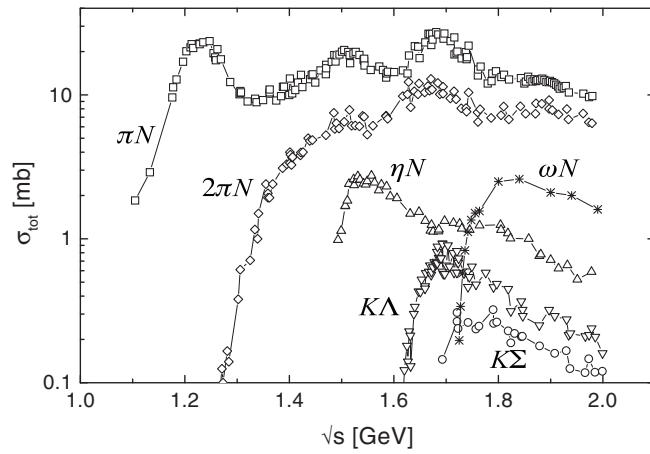


FIG. 1: Total cross sections for the reactions $\pi^- p \rightarrow X$ with X as given in the figure. All data are from ref. [10], the lines are to guide the eye.

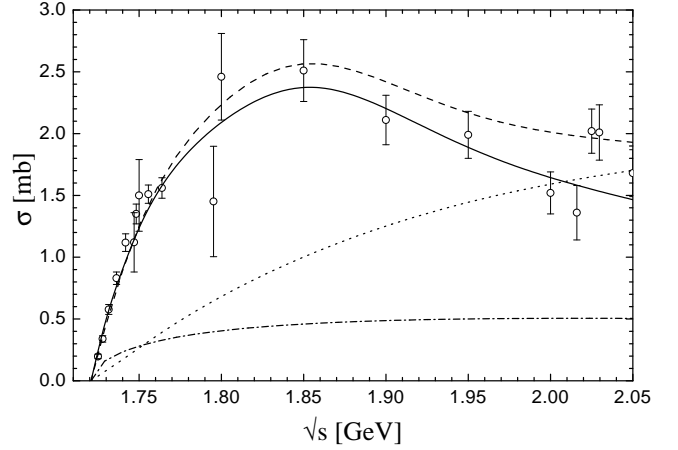


FIG. 2: $\pi^- p \rightarrow \omega n$ total cross section. Solid line: full calculation, dashed: calculation with $g_{NN\omega} = 7.98$, $\kappa_{NN\omega} = -0.12$, dotted: no rescattering, dash-dot: nucleon contribution ignoring rescattering. For the data references, see section IV.

becomes unavoidable and hence the model is extended to also include ωN and $K\Sigma$. As can be seen from fig. 1 for $\sqrt{s} > 1.7$ GeV it is mandatory to take into account the ωN state in a unitary model. Furthermore, ω production on the nucleon represents a possibility to project out $I = \frac{1}{2}$ resonances in the reaction mechanism. However, the ωN channel resisted up to now a theoretical description in line with experiment. Especially the inclusion of nucleon Born contributions [5] overestimated the data at energies above 1.77 GeV and only either the neglect of these diagrams [6, 7] or very soft formfactors [8]¹ led to a rough description of the experimental data. However, none of these models included rescattering effects or a detailed partial-wave analysis of interference effects. As recently pointed out [11] both lead to strong modifications of the observed cross section, see also fig. 2.

The aim of this paper is to present the results of $\pi N \rightarrow$

[†]Supported by DFG and GSI Darmstadt.

*Electronic address: gregor.penner@theo.physik.uni-giessen.de

¹ Note that ref. [8] did not use the correct experimental data, but followed the claim of ref. [9], see section IV.

ωN within a coupled-channel model that simultaneously describes all pion induced data for πN , $2\pi N$, ηN , $K\Lambda$, $K\Sigma$, and ωN . Hence this analysis differs from all other investigations on $\pi N \rightarrow \omega N$ in two respects: First, a larger energy region is considered, which also means there are more restrictions from experiment, and second, the reaction process is influenced by all other channels and vice versa. This leads to strong constraints in the choice of ωN contributions and it is therefore possible to extract them more reliably.

We start with a short review of the model of ref. [4] in section II, where we also present the way the ωN final state is included. Due to the ω intrinsic spin the inclusion of this final state requires an extension of the standard partial-wave decomposition (PWD) method developed for $\pi N/\gamma N \rightarrow \pi N$ and $\gamma N \rightarrow \gamma N$ (see e.g. [4]). Such an extension is provided in section III. In section IV our calculations are compared to the available experimental data and we conclude with a summary.

II. THE MODEL

The scattering equation that needs to be solved is the Bethe-Salpeter (BS) equation for the scattering amplitude:

$$M(p', p; \sqrt{s}) = V(p', p; \sqrt{s}) + \int \frac{d^4 q}{(2\pi)^4} \quad (1)$$

$$\times V(p', q; \sqrt{s}) G_{BS}(q; \sqrt{s}) M(q, p; \sqrt{s}).$$

Here, p (k) and p' (k') are the incoming and outgoing baryon (meson) four momenta. After splitting up the two-particle BS propagator G_{BS} into its real and imaginary part, one can introduce the K -matrix via (in a schematical notation) $K = V + \int V \text{Re} G_{BS} M$. Then M is given by $M = K + i \int M \text{Im} G_{BS} K$. Since the imaginary part of G_{BS} just contains its on-shell part, the reaction matrix T , defined via the scattering matrix $S = 1 + 2iT$, can now be calculated from K after a PWD in J , P , and I via matrix inversion:

$$T(p', p; \sqrt{s}) = \frac{K(p', p; \sqrt{s})}{1 - iK(p', p; \sqrt{s})}. \quad (2)$$

Hence unitarity is fulfilled as long as K is hermitian. For simplicity we apply the so called K -matrix Born-approximation, which means that we neglect the real part of G_{BS} and thus K reduces to $K = V$. For a discussion of the validity of this approximation see ref. [4].

² Note, that the mass of this resonance as given by the references in [14] ranges from 1.8 to 2.08 GeV.

The potential V is built up by a sum of s -, u -, t -channel Feynman diagrams by means of effective Lagrangians which can be found in [4]. The background (non-resonant) contributions to the amplitudes are not added “by hand”, but are consistently created by the u - and t -channel diagrams. Thus the number of parameters is greatly reduced. This holds true for the reaction $\pi^- p \rightarrow \omega N$ in the same way, where we also allowed for the nucleon Born diagrams and a ρ exchange in the t -channel. In our model the following 14 resonances are included: $P_{33}(1232)$, $P_{11}(1440)$, $D_{13}(1520)$, $S_{11}(1535)$, $P_{33}(1600)$, $S_{31}(1620)$, $S_{11}(1650)$, $D_{33}(1700)$, $P_{11}(1710)$, $P_{13}(1720)$, $P_{31}(1750)$, $P_{13}(1900)$, $P_{33}(1920)$, and a $D_{13}(1950)$ (as in [4, 12, 13]) which is listed as $D_{13}(2080)$ by the Particle Data Group [14]².

The resonance ωN Lagrangians we use just extensions of the Lagrangians used in [4] for the $RN\gamma$ transition. For the spin $\frac{1}{2}$ resonances we used the same ωN Lagrangian as for the nucleon ($\omega N \rightarrow R$):

$$\mathcal{L} = \bar{R} \begin{pmatrix} 1 \\ -i\gamma_5 \end{pmatrix} \left(g_1 \gamma_\mu - \frac{g_2}{2m_N} \sigma_{\mu\nu} \partial_\nu \right) N \omega^\mu, \quad (3)$$

where the first coupling is the same one as in [3, 8] since the ω is polarized such that $k'_\mu \omega^\mu = 0$. For the spin $\frac{3}{2}$ resonances we use:

$$\mathcal{L} = \bar{R}^\mu \begin{pmatrix} i\gamma_5 \\ 1 \end{pmatrix} \left(\frac{g_1}{2m_N} \gamma^\alpha + i \frac{g_2}{4m_N^2} \partial_N^\alpha + i \frac{g_3}{4m_N^2} \partial_\omega^\alpha \right) \times (\partial_\alpha^\omega g_{\mu\nu} - \partial_\mu^\omega g_{\alpha\nu}) N \omega^\nu. \quad (4)$$

In both equations the upper operator (1 or $i\gamma_5$) corresponds to a positive and the lower one to a negative parity resonance. For positive parity spin $\frac{3}{2}$ resonances the first coupling also corresponds to the couplings used in [3, 8]. For ambiguities concerning the choice of the resonance nucleon vector meson couplings see ref. [15].

From these couplings the helicity decay amplitudes of the resonances to ωN can be deduced:

$$A_{\frac{1}{2}}^{\omega N} = \pm \frac{\sqrt{E_N \mp m_N}}{\sqrt{m_N}} \left(g_1 + g_2 \frac{m_N \pm m_R}{2m_N} \right) \quad (5)$$

$$A_0^{\omega N} = \pm \frac{\sqrt{E_N \mp m_N}}{m_\omega \sqrt{2m_N}} \left(g_1 (m_N \pm m_R) + g_2 \frac{m_\omega^2}{2m_N} \right)$$

for spin $\frac{1}{2}$ and

$$A_{\frac{3}{2}}^{\omega N} = -\frac{\sqrt{E_N \mp m_N}}{\sqrt{2m_N}} \frac{1}{2m_N} \left(g_3 \frac{m_\omega^2}{2m_N} - g_1 (m_N \pm m_R) + g_2 \frac{m_R^2 - m_N^2 - m_\omega^2}{4m_N} \right)$$

$$\begin{aligned}
A_{\frac{1}{2}}^{\omega N} &= \pm \frac{\sqrt{E_N \mp m_N}}{\sqrt{6m_N}} \frac{1}{2m_N} \left(g_3 \frac{m_\omega^2}{2m_N} \pm g_1 \frac{m_N(m_N \pm m_R) - m_\omega^2}{m_R} + g_2 \frac{m_R^2 - m_N^2 - m_\omega^2}{4m_N} \right) \\
A_0^{\omega N} &= \pm m_\omega \frac{\sqrt{E_N \mp m_N}}{\sqrt{3m_N}} \frac{1}{2m_N} \left(g_1 \mp g_2 \frac{m_R^2 + m_N^2 - m_\omega^2}{4m_R m_N} \mp g_3 \frac{m_R^2 - m_N^2 + m_\omega^2}{4m_R m_N} \right)
\end{aligned} \tag{6}$$

for spin $\frac{3}{2}$ resonances. Again, the upper sign holds for positive and the lower for negative parity resonances. The lower indices correspond to the resonance helicities and are determined by the ω and nucleon spin z -components: $\frac{3}{2}: 1 + \frac{1}{2} = \frac{3}{2}$, $\frac{1}{2}: 1 - \frac{1}{2} = \frac{1}{2}$, and $0: 0 + \frac{1}{2} = \frac{1}{2}$. The resonance ωN decay widths are then given by

$$\Gamma^{\omega N} = \frac{2}{2J+1} \sum_{\lambda=0}^{\lambda=+J} \Gamma_\lambda^{\omega N}, \quad \Gamma_\lambda^{\omega N} = \frac{k' m_N}{2\pi m_R} |A_\lambda^{\omega N}|^2 \tag{7}$$

(upright letters denote the absolute value of the corresponding three momentum). Due to the limited amount of experimental data (we included 114 ωN data points in the fitting procedure, cf. section IV) we tried to minimize the set of parameters and only varied a subset of the ωN coupling constants. In the process of the fitting procedure we allowed for two different couplings (g_1 and g_2) to ωN for those resonances which turned out to couple strongly to this final state, i.e. $P_{11}(1710)$, $P_{13}(1720)$, $P_{13}(1900)$, and $D_{13}(1950)$, and one coupling (g_1) for the $S_{11}(1650)$. Since the usual values for the $NN\omega$ couplings (cf. ref. [4] and references therein) stem from different kinematical regimes than the one examined here, we also allowed these two values to be varied during the fitting procedure. But at the same time, the cutoff value in the vertex formfactor is not allowed to vary freely; instead, the same value is used for all (!) final states, see section IV. It is also important to notice that due to the coupled-channel calculation there are also constraints from all other channels that are compared to experimental data leading to large restrictions in the freedom of choosing the ωN contributions.

III. ω PRODUCTION

Since the orbital angular momentum ℓ is not conserved in, e.g., $\pi N \rightarrow \omega N$ the standard PWD becomes inconvenient for many of the channels that have to be included. Hence we use here a generalisation of the standard PWD method which represents a tool to analyze any meson- and photon-baryon reaction on an equal, uniform footing.

We start with the decomposition of the two-particle c.m. momentum states ($\mathbf{p} = -\mathbf{k}$, $\mathbf{p} = |\mathbf{p}|$) into states with total angular momentum J and $J_z = M$ [16]:

$$|pJM, \lambda_k \lambda_p\rangle = N_J \int e^{i(M-\lambda)\varphi} d_{M\lambda}^J(\vartheta) |p\vartheta\varphi, \lambda_k \lambda_p\rangle d\Omega, \tag{8}$$

where λ_k (λ_p) is the meson (baryon) helicity and the $d_{M\lambda}^J(\vartheta)$ are Wigner functions. The normalization N_J is given by $\sqrt{(2J+1)/(4\pi)}$ and $\lambda = \lambda_k - \lambda_p$. For the incoming c.m. state ($\vartheta_0 = \varphi_0 = 0 \Rightarrow \ell = 0$) one gets $\langle JM, \lambda_k \lambda_p | \vartheta_0 \varphi_0, \lambda_k \lambda_p \rangle \sim \delta_{M\lambda}$, and one can drop the index M . By using the parity property [16] $\hat{P}|J, \lambda\rangle = \eta_k \eta_p (-1)^{J-s_k-s_p} |J, -\lambda\rangle$, where η_k and η_p (s_k and s_p) are the intrinsic parities (spins) of the two particles, the construction of states with a well defined parity is straightforward:

$$\begin{aligned}
|J, \lambda; P\pm\rangle &\equiv |J, +\lambda\rangle \pm \eta |J, -\lambda\rangle \\
\Rightarrow \hat{P}|J, \lambda; P\pm\rangle &= (-1)^{J\pm\frac{1}{2}} |J, \lambda; P\pm\rangle,
\end{aligned} \tag{9}$$

where we have defined

$$\eta \equiv \eta_k \eta_p (-1)^{s_k + s_p - \frac{1}{2}}. \tag{10}$$

They can be used to project out helicity amplitudes with parity $J \pm \frac{1}{2}$:

$$\mathcal{T}_{\lambda'\lambda}^{J\pm} \equiv \langle J, \lambda' | T | J, \lambda; \pm \rangle = \mathcal{T}_{\lambda'\lambda}^J \pm \eta \mathcal{T}_{\lambda'\lambda}^J \tag{11}$$

with

$$\begin{aligned}
\mathcal{T}_{\lambda'\lambda}^J(\sqrt{s}) &\equiv \langle \lambda' | T^J(\sqrt{s}) | \lambda \rangle \\
&= 2\pi \int d(\cos\vartheta) d_{\lambda\lambda'}^J(\vartheta) \langle \vartheta, \varphi = 0, \lambda' | T | 00, \lambda \rangle.
\end{aligned} \tag{12}$$

These helicity amplitudes $\mathcal{T}_{\lambda'\lambda}^{J\pm}$ have definite, identical J and definite, but opposite P . As is quite obvious this method is valid for any meson-baryon final state combination, even cases as e.g. $\omega N \rightarrow \pi\Delta$. In the case of $\pi N \rightarrow \pi N$ the $\mathcal{T}_{\lambda'\lambda}^{J\pm}$ coincide with the conventional partial-wave amplitudes: $\mathcal{T}_{\frac{1}{2}\pm}^{J\pm} \equiv \mathcal{T}_{\ell\pm}$.

IV. COMPARISON WITH EXPERIMENT

For the fitting procedure we modified the data set used in ref. [4] in the following way:

For $\pi N \rightarrow \pi N$ we used the updated single energy partial-wave analysis SM00 [17]. For $2\pi N$, ηN , and $K\Lambda$ we continue to use the same data base as in [4], however, for ηN the data from [18] and for $K\Lambda$ the data from [19] were added. For $K\Sigma$ production we used the total cross section, angle-differential cross section, and polarization data from [20] and from the references to be found in [10].

Furthermore, we have included all the $\pi N \rightarrow \omega N$ data in the literature [21, 22, 23, 24]. At this point we wish

Total	πN	$2\pi N$	ηN	$K\Lambda$	$K\Sigma$	ωN
3.08	3.78	6.95	1.78	2.05	2.43	2.53

TABLE I: χ^2 per degree of freedom from the present calculation for $\pi N \rightarrow X$ with X as given in the table.

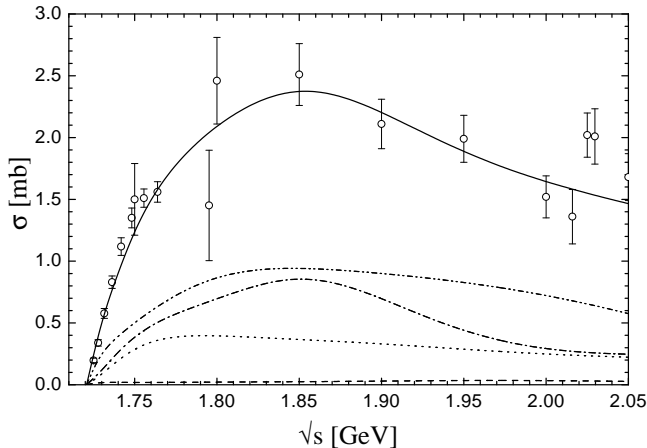


FIG. 3: $\pi^- p \rightarrow \omega n$ total cross section. The contributions of various partial waves are given by $J^P = \frac{1}{2}^- (S_{11})$: dashed, $\frac{1}{2}^+ (P_{11})$: dotted, $\frac{3}{2}^+ (P_{13})$: dash-dot, $\frac{3}{2}^- (D_{13})$: dash-dot-dot (in brackets the πN notation is given). The sum of all partial waves is given by the solid line. For the data references, see text.

to stress that we do not follow the authors of ref. [9] to “correct” the Karami [23] data. The authors of [9] have claimed that the method used in [21, 22, 23] to extract the two-body cross section from the count rates was incorrect. However, a careful reading of ref. [21] reveals that the twobody cross sections were indeed correctly deduced and the peak region of the ω spectral function is well covered even at energies close to the ω production threshold. The incorrect conclusion of ref. [9] can be traced back to the false statement that the experimentalists started with an expression as eqn. (14) in ref. [9]; more details can be found in [25].

The results presented in the following are from ongoing calculations to describe the data of all channels simultaneously (cf. table I). The coupling set used for the presented results leads to an overall χ^2 of 3.08 per degree of freedom (by comparison to a total of 2360 data points).

As can be seen in figs. 3 and 4 our calculation is in line with all total and also with the differential ωN cross sections of refs. [21, 22, 23]³. To get a handle on the angle-differential structure of the cross section for ener-

gies $\sqrt{s} \geq 1.8$ GeV we also extracted angle-differential cross sections from the corrected cosine event distributions given in ref. [24] with the help of their total cross sections. These data points strongly constrain the nucleon u -channel contribution because of the decrease at backward angles, see the end of this section. Moreover, for these energies the contribution of the ρ exchange contribution leads to an increasing forward peaking behavior.

The total ωN cross section (cf. fig. 3) is dominantly composed of two partial waves contributing with approximately the same magnitude $J^P = \frac{3}{2}^- (D_{13})$ and $\frac{3}{2}^+ (P_{13})$, and also a smaller $\frac{1}{2}^+ (P_{11})$ contribution, while the $\frac{1}{2}^- (S_{11})$ partial wave is almost negligible (in brackets the πN notation is given). The main contributions in these partial waves stem from the $D_{13}(1950)$, the $P_{13}(1720)$, the nucleon, and the $P_{11}(1710)$. The $D_{13}(1950)$ is especially interesting, since it is only listed in the PDG [14] at 2.08 GeV, but was already found as an important contribution in πN and $K\Lambda$ channels (cf. [4, 12]) at around 1.95 GeV. In our calculation it turns out to be an important production mechanism as well, in particular at threshold. These findings are also contrary to the conclusions drawn in [23]. Guided by their angle-differential cross sections they excluded any noticeable $J = \frac{3}{2}$ effects and deduced a production mechanism that is dominated by $J = \frac{1}{2}$ contributions. However, our coupled-channel calculation shows that their angle-differential cross sections can indeed be described by dominating $\frac{3}{2}^-$ and $\frac{3}{2}^+$ waves. At the same time, taking into account the $\pi N \rightarrow \pi N$ inelasticities (cf. fig. 5) both a dominating $\frac{1}{2}^-$ and $\frac{1}{2}^+$ mechanism can be excluded.

Due to the coupled-channel calculation, the opening of the ωN channel also becomes visible in the inelasticity of the $\pi N \rightarrow \pi N$ channel. In figs. 5 and 6 the $\pi N \rightarrow \pi N$ inelastic

$$\sigma_{IJP}^{in} = \frac{4\pi}{k^2} \left(J + \frac{1}{2} \right) \left(\text{Im} \mathcal{T}_{\frac{1}{2}\frac{1}{2}}^{IJ\pm} - \left| \mathcal{T}_{\frac{1}{2}\frac{1}{2}}^{IJ\pm} \right|^2 \right) \quad (13)$$

and the $\pi N \rightarrow 2\pi N$ partial-wave cross sections

$$\sigma_{IJP}^{2\pi} = \frac{4\pi}{k^2} \left(J + \frac{1}{2} \right) \left| \mathcal{T}_{\frac{1}{2}\frac{1}{2}}^{IJ\pm} \right|^2 \quad (14)$$

are plotted together with experimental data from SM00 [17] and [26]. A strong $\frac{1}{2}^-$ wave contribution for $I = \frac{1}{2}$ as claimed in [9] would also be in contradiction with the $\frac{1}{2}^-$ inelasticity extracted from the $\pi N \rightarrow \pi N$ partial wave: The $\frac{1}{2}^-$ inelasticity around the ωN threshold is already saturated by the $2\pi N$ and $K\Sigma$ channel; a large ωN contribution would spoil the agreement between calculation and experiment.

Another coupled-channel effect shows up in the total $\pi^- p \rightarrow K^0 \Lambda$ cross section. As can be seen in fig. 7 this channel exhibits a resonance-like behavior for energies $1.67 \text{ GeV} \leq \sqrt{s} \leq 1.73 \text{ GeV}$. However, this structure is

³ The total cross sections given in refs. [21, 22] are actually angle-differential cross sections (mostly at forward and backward neutron c.m. angles) multiplied with 4π .

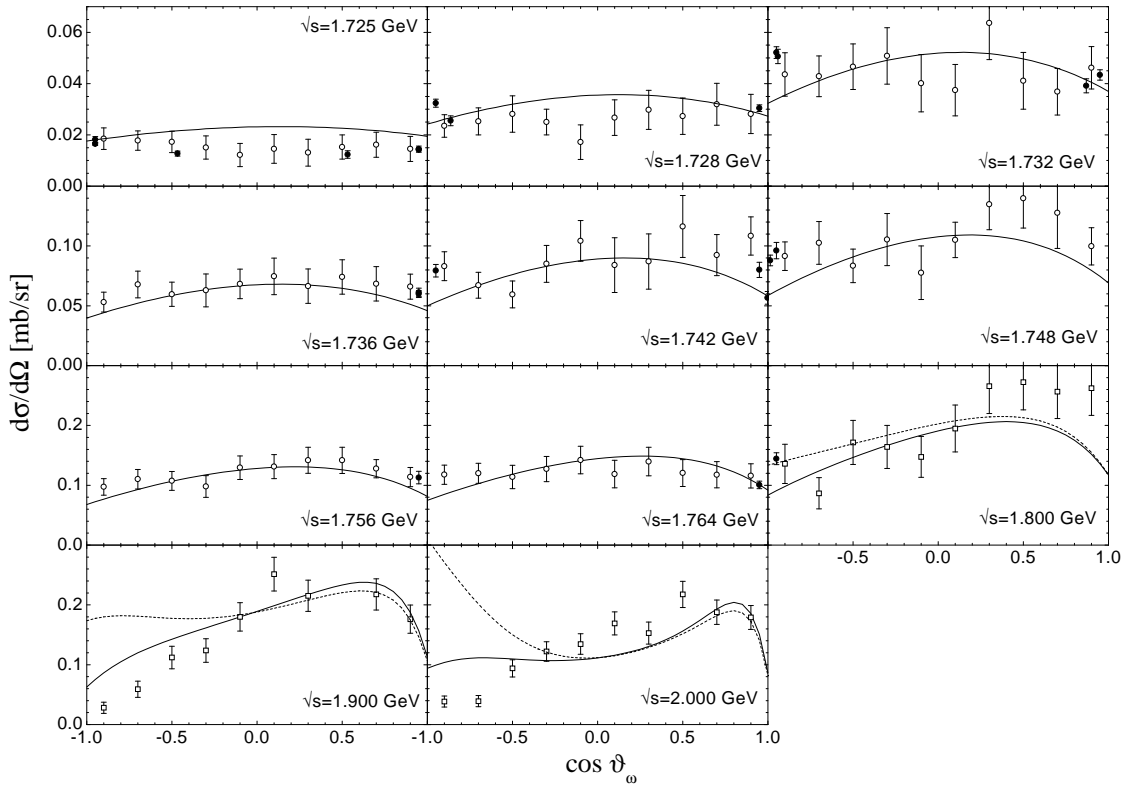


FIG. 4: $\pi^-p \rightarrow \omega n$ differential cross section. Data are from \bullet : [21, 22], \circ : [23], and \square : [24]. For the data points extracted from ref. [24] see text. At energies $\sqrt{s} \geq 1.8$ GeV also a calculation with $g_{NN\omega} = 7.98$, $\kappa_{NN\omega} = -0.12$ is shown (dashed line).

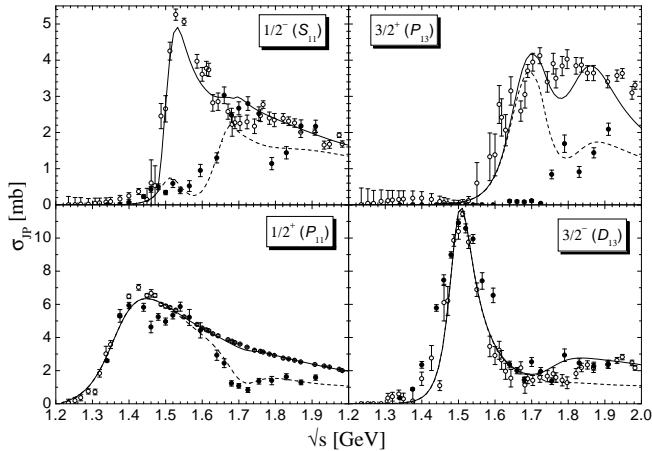


FIG. 5: $\pi N \rightarrow \pi N$ inelastic (\circ as extracted from SM00 [17], calculation: solid line) and $\pi N \rightarrow 2\pi N$ partial-wave cross sections (\bullet as extracted by [26], calculation: dashed line), both for $I = \frac{1}{2}$. See refs. [4] and [27] for the discrepancy of $\pi N \rightarrow 2\pi N$ in the $\frac{3}{2}^+(P_{13})$ partial wave between 1.55 and 1.73 GeV.

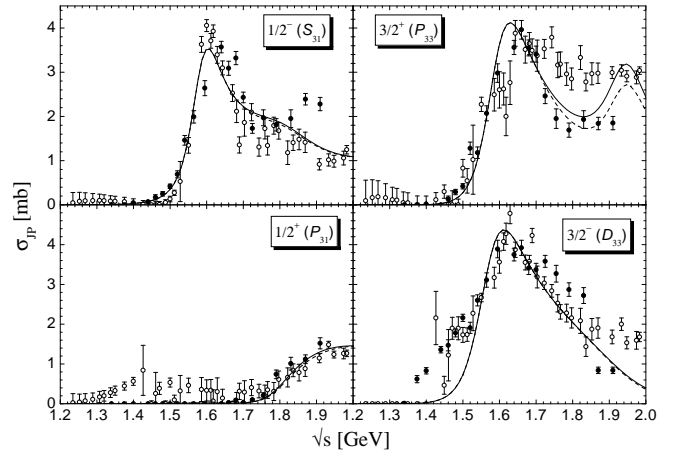


FIG. 6: $\pi N \rightarrow \pi N$ inelastic (\circ as extracted from SM00 [17], calculation: solid line) and $\pi N \rightarrow 2\pi N$ partial-wave cross sections (\bullet as extracted by [26], calculation: dashed line), both for $I = \frac{3}{2}$.

also caused by the opening of two new channels, that take away the flux in the $\frac{1}{2}^-$ and $\frac{3}{2}^+$ partial waves. First, around 1.69 GeV the $K\Sigma$ channel opens up with a strong

$IJ^P = \frac{1}{2}1^-$ contribution. Second, around 1.72 GeV ωN opens up with a small $\frac{1}{2}\frac{1}{2}^-$ but a strong $\frac{1}{2}\frac{3}{2}^+$ wave. The $\pi N \rightarrow K\Sigma$ cross sections are shown in fig. 8. The pure $I = \frac{3}{2}$ channel $\pi^+p \rightarrow K^+\Sigma^+$ is strongly dominated by

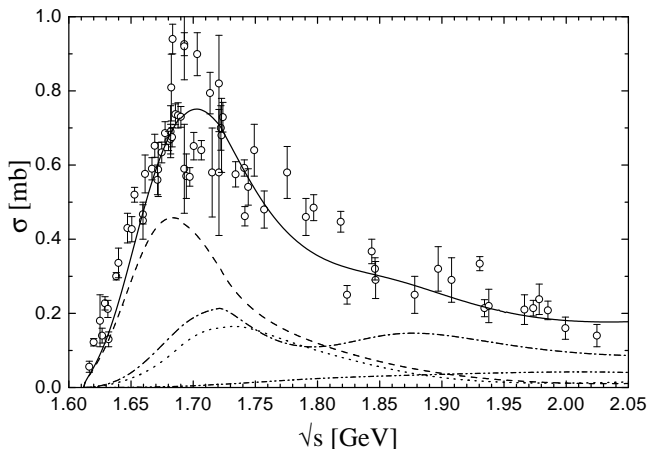


FIG. 7: $\pi^- p \rightarrow K^0 \Lambda$ total cross section. See fig. 3 for the notation. For the data references, see text.

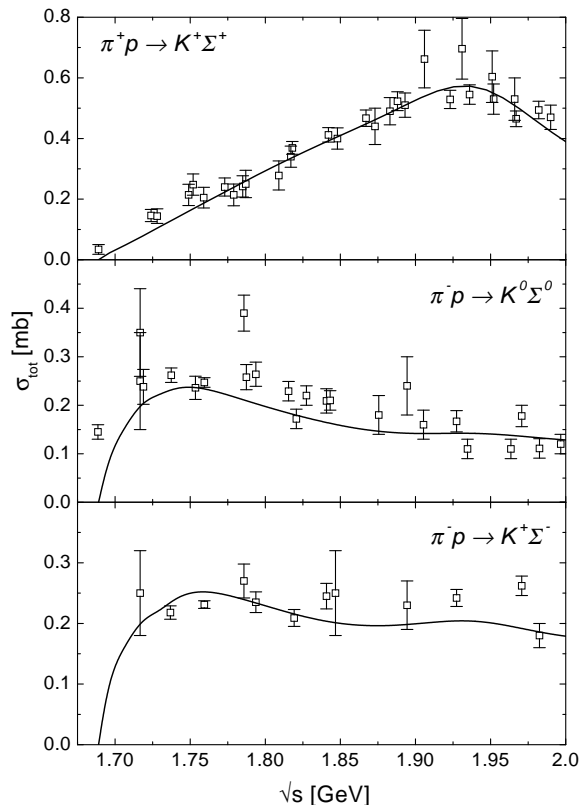


FIG. 8: $\pi N \rightarrow K \Sigma$ total cross sections.

a $\frac{3}{2}\frac{3}{2}^+$ wave and also becomes visible in the $\frac{3}{2}\frac{3}{2}^+$ πN -inelasticity (cf. fig. 6), while the other two channels $\pi^- p \rightarrow K^0 \Sigma^0 / K^+ \Sigma^-$ show the strong $\frac{1}{2}\frac{1}{2}^-$ -wave rise just above threshold.

As mentioned above we also allowed for the nucleon Born contributions in $\pi N \rightarrow \omega N$ usually leading to an overestimation of the total cross section at higher ener-

$L_{2I2J}^{\pi N}$	M	Γ_{tot}	$\Gamma_0^{\omega N}$	$\Gamma_{\frac{1}{2}}^{\omega N}$	$\Gamma_{\frac{3}{2}}^{\omega N}$	$\Gamma^{\omega N}$	$\Gamma^{\omega N}$ of [2]
$S_{11}(1650)$	1677.5	177	-0.224 ^a	0.0 ^{ab}	—	—	—
$P_{11}(1710)$	1786.3	686	76	69	—	145	0.0 ^{+5.3} _{-0.0}
$P_{13}(1720)$	1722.5	252	0.05	0.11	1.18	0.67	0.0 ^{+1.7} _{-0.0}
$P_{13}(1900)$	1951.0	585	21	0	226	123	20.3 ^{+34.8} _{-0.0}
$D_{13}(1950)$	1946.0	948	162	0	289	226	39.7 ^{+56.3} _{-21.2}

TABLE II: Masses, total and ωN widths (see 7) for $I = \frac{1}{2}$ resonances coupling to ωN . All values are given in MeV. For the ωN widths of ref. [2], we also cite the upper and lower values of their extracted ranges. ^aThe couplings g_1, g_2 are given. ^bNot varied in the fit, see text.

gies. As can be seen in fig. 2, the inclusion of rescattering is mandatory to be able to describe the energy dependent behavior of the total $\pi N \rightarrow \omega N$ cross section: When we apply our best parameter set to a tree level calculation, i.e. “rescattering” is only taken into account via an imaginary part in the denominator of the resonance propagators, the calculation results in the dotted line, which is far off the experimental data. This shows the importance of “off-diagonal” rescattering such as $\pi N \rightarrow \pi N \rightarrow \omega N$ or $\pi N \rightarrow K \Lambda \rightarrow \omega N$.

The values of the $NN\omega$ couplings are mainly determined by the backward angle-differential cross section at higher energies. During the fitting procedure these couplings resulted in $g_1 = 4.50$ and $\kappa = g_2/g_1 = -0.70$. The total cross section exhibits almost the same behavior when we use the values from [4] ($g_1 = 7.98$ and $\kappa = -0.12$, see the dashed line in fig. 2), however, for energies above $\sqrt{s} = 1.8$ GeV the angular dependence (see the dashed line in fig. 4) is not in line with experiment anymore. The NN -meson cutoff value used for all (!) s - and u -channel diagram vertices (hence also for the $NN\omega$ vertex) resulted in $\Lambda_N = 1.15$ GeV; the cutoff function is the same as in [4]: $F(q^2) = \Lambda_N^4 / (\Lambda_N^4 + (q^2 - m_N^2)^2)$.

For the other background contribution in the ωN production, i.e. the ρ exchange, we used the couplings $g_{\omega\rho\pi} = 2.056$ (extracted from the $\omega \rightarrow \rho\pi \rightarrow \pi^+\pi^-\pi^0$ width), $g_{NN\rho} = 5.56$, and $\kappa_{NN\rho} = 1.58$ – the latter values were extracted from the fit and are the same as in calculating πN elastic scattering.

In table II the resonance properties of those resonances which couple to ωN are presented. In contrast to [2, 3, 8] we also find strong contributions from the $P_{11}(1710)$ and the $P_{13}(1720)$ resonances, where the latter one is located just above the ωN threshold of 1.72084 GeV. We can also compare our $S_{11}(1650)$ and $P_{13}(1720)$ couplings to the one from [3, 8] if we choose to take the same width for the P_{13} , but only use the first coupling (g_1). While we find only a small S_{11} coupling of $g_1 = -0.22$, but a large value of $g_1 = 29.3$ for the P_{13} , [3, 8] found -2.56 and 3.17 , resp.. However, as is clear from the discussion above, a strong P_{13} and a small S_{11} are mandatory results of our coupled-channel analysis. For the $P_{11}(1710)$, $P_{13}(1720)$, and $D_{13}(1950)$ also a comparison to the VMD

(vector meson dominance) predictions of ref. [6] is possible. The authors of ref. [6] used different photon helicity amplitude analyses to extract ranges for the $RN\omega$ transition couplings under the assumption of strict VMD. Using their notation we find from our widths the following couplings: $P_{11}(1710)$: 6.3 (0 – 1.22), $P_{13}(1720)$: 15.6 (0 – 5.0), and $D_{13}(1950)$: 2.3 (0 – 2.6). In brackets, their VMD ranges are given. Due to the large uncertainties in the photon helicity amplitudes, which are the input to the calculation of [6], it is impossible to draw any conclusion on the validity of strict VMD for these resonances.

V. CONCLUSIONS AND OUTLOOK

In this paper we have included the ωN final state into our coupled-channel model and have investigated whether it is possible to find a way to describe the hadronic ωN data. The results of our calculations show that for a description of the reaction $\pi^- p \rightarrow \omega N$ in line with experimental data a unitary, coupled-channel cal-

ulation is mandatory, and the resulting amplitude is mainly composed of $IJ^P = \frac{1}{2}\frac{3}{2}^- (D_{13})$, $\frac{1}{2}\frac{3}{2}^+ (P_{13})$, and $\frac{1}{2}\frac{1}{2}^+ (P_{11})$ contributions, where the $\frac{1}{2}\frac{3}{2}^-$ dominates over the complete considered energy range.

The next step in our investigation of nucleon resonance properties within our coupled-channel K -matrix model will naturally be the inclusion of photon induced data to further pin down the extracted widths and masses. The results of this study and also more details about the calculation presented here will be published soon [13].

Furthermore, since the partial-wave formalism is now settled, the inclusion of additional final states, in particular for a more sophisticated description of the $2\pi N$ final state, as ρN or $\pi\Delta$ is rather straightforward. Also, by the inclusion of several e.g. ρN final states with different masses m_ρ the width of the ρ meson (and similarly for the Δ) can also be taken into account. Finally, investigations concerning the inclusion of spin $\frac{5}{2}$ resonances are underway.

-
- [1] F.X. Lee and D.B. Leinweber, Nucl. Phys. **B73**, 258 (1999).
- [2] S. Capstick and W. Roberts, Phys. Rev. D **47**, 2004 (1993), *ibid.* D **49**, 4570 (1994), S. Capstick and N. Isgur, Phys. Rev. D **34**, 2809 (1986).
- [3] D.O. Riska and G.E. Brown, Nucl. Phys. **A679**, 577 (2001).
- [4] T. Feuster and U. Mosel, Phys. Rev. C **58**, 458 (1998), T. Feuster and U. Mosel, Phys. Rev. C **59**, 460 (1999).
- [5] F. Klingl, Ph.D. thesis, University of Munich, Hieronymus, Munich 1998.
- [6] M. Post and U. Mosel, Nucl. Phys. **A688**, 808 (2001).
- [7] M. Lutz, G. Wolf, and B. Friman, Nucl. Phys. **A661**, 526c (1999) and *Proceedings of the International Workshop XXVIII on Gross Properties of Nuclei and Nuclear Excitations: Hirschegg, Austria, 16-22 Jan. 2000*, Editors: M. Buballa, B.-J. Schaefer, W. Nörenberg, J. Wambach, GSI; e-Print ArXive: [nuc1-th/0003012](https://arxiv.org/abs/nuc1-th/0003012).
- [8] A.I. Titov, B. Kämpfer, and B.L. Reznik, e-Print ArXive: [nuc1-th/0102032](https://arxiv.org/abs/nuc1-th/0102032).
- [9] C. Hanhart and A. Kudryavtsev, Eur. Phys. J. A **6**, 325 (1999).
- [10] H. Höhler, *Landolt-Börnstein*, Vol. 9, Springer, Berlin 1983.
- [11] G. Penner and U. Mosel, *Proceedings of the Workshop on The Physics of Excited Nucleons, NStar 2001*, World Scientific 2001.
- [12] T. Mart and C. Bennhold, Phys. Rev. C **61**, 012201(R) (1999).
- [13] G. Penner and U. Mosel, to be published.
- [14] D.E. Groom et al., Eur. Phys. J. C **15**, 1 (2000).
- [15] M. Post, S. Leupold, and U. Mosel, Nucl. Phys. **A689**, 753 (2001).
- [16] M. Jacob and G.C. Wick, Ann. Phys. **7**, 404 (1959).
- [17] M.M. Pavan, R.A. Arndt, I.I. Strakovsky, and R.L. Workman, Phys. Scripta **T87** 62 (2000), e-Print ArXive [nuc1-th/9807087](https://arxiv.org/abs/nuc1-th/9807087), R.A. Arndt, I.I. Strakovsky, R.L. Workman, and M.M. Pavan, Phys. Rev. C **52**, 2120 (1995), updates available via: <http://gwadac.phys.gwu.edu/>.
- [18] T.W. Morrison, Ph.D. thesis, The George Washington University, 1999, to be published.
- [19] O.I. Dahl, L.M. Hardy, R.I. Hess, J. Kirz, D.H. Miller, and J.A. Schwartz, Phys. Rev. **163**, 1430 (1967); O. Goussu, M. Sen, B. Ghidini, S. Mongelli, A. Romano, P. Waloschek, and V. Alles-Borelli, Il Nuov. Cim. **XLII A**, 607 (1966).
- [20] J. Haba, T. Homma, H. Kawai, M. Kobayashi, K. Miyake, T.S. Nakamura, N. Sasao, and Y. Sugimoto, Nucl. Phys. **B299**, 627 (1988), Erratum *ibid.* **B308**, 948 (1999).
- [21] D.M. Binnie et al., Phys. Rev. D **8**, 2789 (1973).
- [22] J. Keyne, D.M. Binnie, J. Carr, N.C. Debenham, A. Duane, D.A. Garbutt, W.G. Jones, I. Siotis, and J.G. McEwen, Phys. Rev. D **14**, 28 (1976).
- [23] H. Karami, J. Carr, N.C. Debenham, D.A. Garbutt, W.G. Jones, D.M. Binnie, J. Keyne, P. Moissidis, H.N. Sarma, and I. Siotis, Nucl. Phys. **B154**, 503 (1979).
- [24] J.S. Danburg, M.A. Abolins, O.I. Dahl, D.W. Davies, P.L. Hoch, J. Kirz, D.H. Miller, and R.K. Rader, Phys. Rev. D **2**, 2564 (1970).
- [25] G. Penner and U. Mosel, submitted to Eur. Phys. J. A, e-Print ArXive: [nuc1-th/0111024](https://arxiv.org/abs/nuc1-th/0111024).
- [26] D.M. Manley, R.A. Arndt, Y. Goradia, and V.L. Teplitz, Phys. Rev. D **30**, 904 (1984).
- [27] D.M. Manley and E.M. Saleski, Phys. Rev. D **45**, 4002 (1992).